Aeroacoustics Conferences
June 14-17, 2022, Southampton, UK
28th AIAA/CEAS Aeroacoustics 2022 Conference

10.2514/6.2022-3028

Acoustic Source Characterization of an Installed GE F404 Engine Using Near-field Acoustical Holography

Logan T. Mathews[1], Kent L. Gee[2], and Kevin M. Leete[3]
Brigham Young University, Provo, Utah, 84602

Alan T. Wall[4]
Air Force Research Laboratory, Wright-Patterson AFB, Ohio, 45433

Acoustic source characterization of full-scale supersonic jets remains a vital component of understanding jet noise. Identification of fundamental characteristics such as source location(s) and directivity will better inform physical understanding, noise models, engine design, and noise reduction technologies. This paper investigates an installed F404-GE-103 engine as an acoustic source using statistically optimized near-field acoustical holography (SONAH) for engine conditions ranging from 50% thrust to afterburner. Partial field decomposition is used to characterize the coherent nature of the source as a function of frequency. Spatiospectral reconstructions along the nozzle lipline show distinct behavior at different engine conditions. Lower engine conditions show two energetic spatial regions along the lipline from 200-300 Hz. Three distinct local maxima are observed at AB. These maxima are correlated with other studies about supersonic jet noise sources in the literature. Mach wave radiation is thought to be tied to the first two local maxima, which occur throughout the shear layer, ending ahead of the approximate supersonic core tip. The third, lower-frequency maximum is proposed to be correlated with noise from large-scale turbulence structures.

Downloaded by Kent Gee on June 13, 2022 | http://arc.aiaa.org | DOI: 10.2514/6.2022-3028

I. Nomenclature

MARP	=	microphone array reference point
x	=	distance downstream of jet nozzle exit
y	=	horizontal distance from jet centerline
D_e	=	jet nozzle exit diameter
L_c	=	potential core length
L_s	=	supersonic core length
PF	=	partial field
LM	=	local maximum
NAH	=	nearfield acoustical holography
SONAH	=	statistically optimized nearfield acoustical holography
MIL	=	full military power (100% thrust)
AB	=	full afterburner (~160% thrust)
BSN	=	broadband shock-associated noise
LSN	=	large-scale turbulence structure radiated noise
FSN	=	fine-scale turbulence structure radiated noise
MWR	=	Mach wave radiation
TTR	=	total temperature ratio

[1] Graduate Student, Department of Physics and Astronomy, AIAA student member
[2] Professor of Physics, Department of Physics and Astronomy, AIAA senior member
[3] Graduate Student, Department of Physics and Astronomy, AIAA student member
[4] Research Physicist, Battlespace Acoustics Branch, 2610 Seventh St., Bldg. 441, Wright-Patterson AFB, OH 45433, AIAA member

Copyright © 2022 by the authors. Published by the American Institute of Aeronautics and Astronautics, Inc., with permission.

LES = large-eddy simulation

II. Introduction

Despite decades of research into acoustic source characteristics of supersonic jets[1–4], significant properties remain ill-defined. While substantial progress has been made over recent years with lab-scale and full-scale supersonic jets, as well as computational simulations, many fundamental source questions remain unsatisfied. In particular, understanding of full-scale, installed, high-temperature ratio afterburning jets requires further research to develop physical understanding of noise generation mechanisms, formulate physics-based methods for predicting noise, and for informing the design of noise reduction technologies.

In referring to jet noise phenomena, it is useful to reference elementary regions of the jet flow. Extending from the nozzle exit downstream is the potential core, a region of relatively constant velocity fluid. The potential core tapers off gradually as the turbulent mixing layer, caused by the velocity shear between the jet and ambient atmosphere, slowly grows and eventually spans the full cross-section of the plume. The potential core exists for both sub- and supersonic jets. In a supersonic jet, the flow is supersonic throughout the potential core and a portion of the flow remains supersonic beyond the potential core. This region, called the supersonic core, also eventually terminates somewhere downstream of the potential core, whereupon the flow is subsonic throughout its cross-section. The lengths of the potential and supersonic cores are denoted as L_c and L_s, respectively.

Directly measured values for L_c and L_s are generally unavailable for full-scale, highly heated supersonic jets, so reliance upon data from analogous lab-scale and simulated jets is required. These quantities are expected to differ based on jet total temperature ratio (TTR), where TTR ≈ 3 is similar to a military jet operating at maximum dry power (MIL) and TTR ≈ 7 is similar to an afterburning condition (AB). A recent study by Leete *et al.*[5] for a simulated, supersonic, TTR = 7.0 jet indicated values for L_c and L_s of $x/D_e \approx 7.2$ and $x/D_e \approx 12.7$, respectively. Chen *et al.*[6] found similar potential core lengths for rectangular lab-scale supersonic jets with $L_c \approx 7.5$-$8.2\ D_e$ and $L_c \approx 6.3\ D_e$ for TTR = 4.0 and 7.0, respectively. Additionally, Tang *et al.*[7] showed a L_c of $x/D_e \approx 8.41$ for a supersonic oxygen jet using a CFD model. Baars *et al.*[8] found L_c for an unheated, Mach 3 supersonic lab-scale jet to be approximately $x/D_j \approx 6.3$ and a L_s of about $x/D_j \approx 13$. A numerical simulation of a Mach 1.65, TTR = 2.9 jet similar to an F404 by Liu *et al.*[9] showed a L_c of $x/D_e \approx 6.4$-7.2 and L_s of $x/D_e \approx 12$-12.4. The values of L_c and L_s for MIL-like conditions seem to be slightly less than AB, but are still relatively close. Thus, the lengths of the potential and supersonic cores noted by Leete *et al.*[5] do seem consistent with what has been found in other studies of jets with at least a similar range of flow parameters and will be used to guide the interpretation of results.

The location and extent of the source region in full-scale, supersonic jets has received appreciable recent attention. The acoustic source is noncompact, presenting the possibility for radiation from distinct flow regimes. Local flow properties evolve with movement downstream, and thus different source mechanisms are present throughout the source region. Efforts to characterize source mechanisms in sub- and supersonic jets have resulted in four primary mechanisms of noise generation: broadband shock-associated noise (BSN), noise generated by large-scale turbulence structures (LSN), noise generated by fine-scale turbulence structures (FSN), and Mach wave radiation (MWR). A comprehensive study of all four of these mechanisms concurrently has been rare in the literature. Instead, most studies focus on one or two of these mechanisms. Tam *et al.*[10,11] and Viswanathan[12], among others, have investigated and proposed models for FSN and LSN in jet noise. These mechanisms are thought to originate from different locations and structure types within the flow. Viswanathan showed that noise attributable to large-scale structures originated in the shear layer of a high-speed jet, grew exponentially along the potential core, and finally decayed downstream of L_c. Recent investigations by Vaughn *et al.*[13], Liu *et al.*[14], Prasad and Morris[15], and Chen *et al.*[6] into high-total temperature ratio (TTR) jets similar to MIL and AB conditions have attributed unidirectional radiation from throughout the shear layer to MWR, distinct from LSN which radiates at farther aft angles.

Localization of the acoustic source in jets and attempts to relate its location to flow regions have elicited much research, both historical and modern. Early efforts by Potter[16], Nagamatsu *et al.*[2,17], and Eldred[18] focused on the region of maximum sound power production. A plotting error in the Potter report, recently discovered by Gee[19], resulted in two different conclusions which both persisted throughout the literature. Whereas the jet noise community has followed the Nagamatsu *et al.* rendering of Potter's results which places the majority of power production upstream of L_s, the rocket noise community has favored the Eldred model, which attributes nearly 50% of total power production downstream of L_s. The correct findings from Potter (which was used by Nagamatsu *et al.*) indicated that the region of maximum sound power production existed just upstream of L_s. A more recent study of a high-temperature ratio supersonic jet from a large-eddy simulation (LES)[14,20,21] by Leete *et al.*[22] showed that more than ~50% of

Downloaded by Kent Gee on June 13, 2022 | http://arc.aiaa.org | DOI: 10.2514/6.2022-3028

sound power was produced upstream of L_c (peaking just before L_c) when the peak directivity angle is controlled by MWR, with the remaining majority of power coming from between L_c and L_s. Only ~<10% of sound power was shown to be produced beyond L_s. This verifies earlier findings that most of the sound power is produced upstream of L_s.

Investigating the same simulation, Leete *et al.*[5] connected radiated noise in the field to regions in the flow. Coherence results indicated three primary source regions: the first originating from the flow upstream of the potential core ($x < 7.2\ D_e$), the second in the region downstream of the potential core but before the end of the supersonic core ($7.2\ D_e < x < 12.7\ D_e$), and the third region downstream of the potential core ($x > 13\ D_e$). Additionally, Leete *et al.*[10] found evidence of these three source regions in a full-scale afterburning jet using an acoustical holography-based coherence analysis along the nozzle lipline.

Regarding distinct source regions for different noise phenomena, Liu *et al.*[23] also noted three distinct source regions in LES of supersonic jets. In another paper, Liu *et al.*[14] investigated noise radiated from a simulated Mach 1.5, TTR = 7.0 jet, and found that two distinct lobes were present around the maximum radiation direction. These two features radiated in slightly different directions. Mach wave radiation, consisting of higher frequencies, radiated at lesser angles relative to the inlet from farther upstream and LSN consisting of lower frequencies radiated further aft angles and from farther downstream. Chen *et al.*[6] also noted similar effects, with a lower-frequency component radiating between 140-160 degrees and a higher frequency component radiating at around 120 degrees; these were associated with LSN and MWR, respectively. Notably, many studies have generally combined the phenomena of LSN and MWR, citing that MWR is the mechanism by which large-scale structures radiate noise. Liu *et al.*[14] and Prasad and Morris[15] showed that this connection likely stems from cold or low TTR jet studies, where MWR and LSN are largely combined. For higher TTR flows, MWR separates from LSN, radiating at lesser angles relative to the inlet.

The difference in radiation angles from different flow regions and source mechanisms is likely due to their physical location in the plume. Mean convective velocity in the shear layer should decrease with movement downstream, so sound emanating from different locations should result in radiated sound emanating in different directions. Like observations made by Liu *et al.* for simulated jets, many studies of full-scale supersonic jet noise have seen evidence of multiple radiation lobes/angles, which can be investigated in light of distinct source regions. Leete *et al.*[24] found evidence of multiple different lobes radiated in the field and used near-field acoustical holography (NAH) to determine the locations along the jet centerline at which three of these lobes appeared to originate.

A recent study by Vaughn *et al.* [13] used an event-based beamforming method based on shock-related events to group and localize related noise phenomena for a full-scale, high-performance jet. These groups were presumed to be associated with BSN, FSN, LSN, and MWR based on their locations and behaviors. Results for AB showed unidirectional radiation originating throughout the shear layer, with directional LSN originating far downstream, aft of the unidirectional radiation. These were associated with MWR and LSN, respectively. A recent study by Schmidt *et al.*[25] of LES jets showed two distinct sound production mechanisms: Kelvin-Helmholtz (KH)-type instability waves, which begin early in the flow and grow throughout the shear layer, and Orr-type instability waves, which occur farther downstream. Given that the KH-type waves are associated with higher speed convective velocities, it would be expected that these would radiate at lesser angles relative to upstream than Orr-type waves. Thus, phenomenologically, KH-type waves could be linked with MWR originating farther upstream, and Orr-type waves with LSN, originating farther downstream and radiating at farther aft angles. Prasad and Morris, on a simulation of a model F404 nozzle at TTR = 2.5, indicated a growth of KH-type instabilities throughout the shear layer with strong MWR, while the deceleration of the flow after L_c leads to the onset of noticeable LSN.

Several other studies have characterized various acoustic properties of the F404 engine, including Seiner *et al.* [26], Greska *et al.* [27], Greska and Krothapalli [28], and Murray and Jansen [29]. Podboy *et al.*[30] conducted phased-array measurements over a limited aperture to locate apparent acoustic sources for an uninstalled F404 operating at various engine conditions. The dominant noise source as detected from the sideline was shown to be about 5 diameters downstream of the nozzle exit at 300 Hz. In addition to this body of research on the F404, numerous other studies have been conducted on full-scale, high-performance military engines[24,31–40].

The purpose of this paper is to investigate key source characteristics of an installed F404-GE-103 engine at engine conditions ranging from 50% thrust to maximum afterburner (AB) using statistically optimized near-field acoustical holography techniques to characterize the acoustic source. Results of the partial field decomposition are used to investigate the density of dominant noise sources by frequency. The source is shown to consist of relatively few energetic, coherent sources below 100 Hz, while higher frequencies up to 1 kHz require increasingly more partial fields to reconstruct most of the energy. The distribution of acoustic pressure sources is investigated using

Downloaded by Kent Gee on June 13, 2022 | http://arc.aiaa.org | DOI: 10.2514/6.2022-3028

spatiospectral reconstructions along the nozzle lipline. Efforts are made to connect observed phenomena with L_c and L_s. Relative local maxima observed in the reconstructions for AB correlate closely with recent source observations of high-temperature ratio, supersonic, full-scale and simulated jets in the literature.

III. Methods

A. Measurement Overview

The Boeing/Saab T-7A Red Hawk is an advanced jet trainer aircraft developed for the United States Air Force and is powered by the F404-GE-103 afterburning turbofan engine. This engine is a further development in the F404 family, which has been the subject of numerous acoustic studies[9,41,42]. The engine has nominal thrust specifications of 48.9 kN (11,000 lb) at full power (MIL) and 78.7 kN (17,700 lb) with full afterburner (AB). Measurements were made in six runs of five different engine conditions, 75% N2 (25% thrust), 82% N2 (50% thrust), 88% N2 (75% thrust), military power (MIL, 100% thrust), and maximum afterburner (AB, ~160% thrust). Engine condition percentages reported throughout this paper will refer to the percentage of thrust for conditions (50% thrust, 75% thrust, etc.). The exit diameter for 50% thrust through MIL is expected to be nominally similar and was measured to be D_e = 0.51 m. The exit diameter at the AB condition has been found to be nominally D_e = 0.62 m, based on image analysis. This parameter is subject to change but is presumed to be accurate to within 5% of the actual value.

Figure 1. Photo of T-7A aircraft measurement with ground-based imaging array highlighted in yellow.

Acoustic data were obtained from an extensive measurement of the T-7A aircraft at Holloman Air Force Base in August 2019. Details of the measurement are given by Leete *et al.*[43] Numerous microphone arrays were deployed to measure the aircraft; however, this study focuses on a 120-element ground array placed near the aircraft, shown in Fig. 1. A schematic of this array is shown in Fig. 2 and is referred to as the imaging array for its primary use in imaging-type analyses such as acoustical holography and beamforming. The array spans a nearly 70 m aperture, from 15 m in front of the exit plane to ~55 m downstream of the nozzle exit. To produce such an aperture with 120 microphones, element spacing was varied based on expected frequency content. The portion of the array near and ahead of the microphone array reference point (MARP, located at x = 3.96 m) was configured with relatively close microphone spacing, resulting in a higher spatial Nyquist frequency to accommodate broadband shock-associated noise (BSN) and other noise with significant high-frequency content. Notably, elements far downstream were given much greater spacing because of the anticipated dominance of lower frequency MWR or LSN. This allowed for a greater aperture to be captured with a limited number of microphones, while not sacrificing fidelity in areas where higher frequency content is expected to be prevalent.

Downloaded by Kent Gee on June 13, 2022 | http://arc.aiaa.org | DOI: 10.2514/6.2022-3028

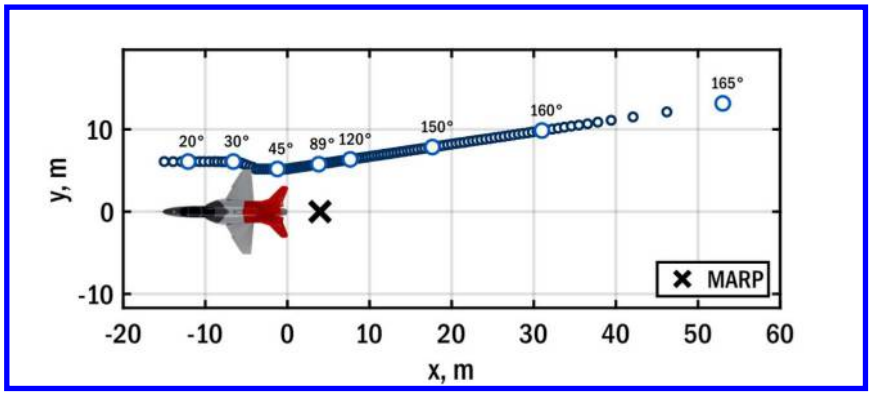

Figure 2. Schematic of the imaging array layout for the T-7A measurement.

B. Analysis Methods

Statistically optimized near-field acoustical holography (SONAH) is an inverse method developed for a variety of acoustic problems and has been applied to jet noise sources[37,44–46]. An overview of the SONAH process is given here, but more detailed descriptions of the SONAH process may be found in Refs. [47,48], with application to jet-noise-specific problems in Refs. [24,37]. The SONAH process is a method of leveraging a limited measurement array (often referred to as the hologram) to reconstruct acoustic properties at locations of interest. It is assumed that the acoustic behavior at the hologram can be represented as a linear combination of wavefunctions (in a matrix $\mathbf{A}$) which satisfies the linear equation

$$\boldsymbol{Ac} = \boldsymbol{p_h}, \tag{1}$$

where $\boldsymbol{c}$ is a vector of unknown coefficients and $\mathbf{p_h}$ is a vector of measured complex pressures at the hologram. The SONAH algorithm applied in this paper uses an equivalent wave model (EWM) based on a set of cylindrical wave functions defined relative to an axis along the jet centerline. These basis functions, comprised of Hankel functions for the radial component and complex exponentials for the azimuthal and x dependence, are given by

$$\Psi_{l,k_x}(r,\phi,x) \equiv \frac{H_l^{(1)}(k_r r)}{H_l^{(1)}(k_r r_0)} e^{il\phi} e^{ik_x x}, \qquad r \geq r_0, \tag{2}$$

where the radial wavenumber, k_r, is determined by

$$k_r = \begin{cases} \sqrt{k^2 - k_x^2}, & |k| \geq |k_x|, \\ i\sqrt{k_x^2 - k^2}, & |k| < |k_x|, \end{cases} \tag{3}$$

where the second case accommodates evanescent radiation, thus accomplishing the near-field portion of SONAH.

In this paper, we only consider the $l = 0$ (axisymmetric) case for the set of wavefunctions. Due to the measurement array being confined to the ground, representation of higher-order azimuthal modes would be inaccurate. In addition, Leete *et al.*[49] showed favorable azimuthal coherence up to several hundred hertz for a high-performance military

Downloaded by Kent Gee on June 13, 2022 | http://arc.aiaa.org | DOI: 10.2514/6.2022-3028

jet, lending credence to the inclusion of only the axisymmetric wavefunctions for this paper. The complete EWM is then formed as the matrix **A**, given as

$$\boldsymbol{A} = \begin{bmatrix} \Psi_1(r_{h1}) & \cdots & \Psi_1(r_{hm}) \\ \vdots & \ddots & \vdots \\ \Psi_N(r_{h1}) & \cdots & \Psi_N(r_{hm}) \end{bmatrix}, \tag{4}$$

where N is the number of wavefunctions used and m is the number of measurement (hologram) points. Sufficient wavefunctions are generated to construct an effectively complete basis over a source-free region of interest. While no analytical criterion exists for determining what constitutes a complete basis in SONAH, a complete basis is effectively achieved when the addition of additional wavefunctions produces no change in the solution. Additional discussion on the selection of wavefunctions in **A** is given by Hald[48]. In essence, the matrix **A** is a transfer matrix from the hologram to a reference surface very close to the jet centerline. The inverse problem is then formulated as

$$\boldsymbol{c} = \boldsymbol{A}^{-1}\boldsymbol{p_h}. \tag{5}$$

In practice, **A** is nonsquare and the inversion is nontrivial. Depending on the dimensions of **A**, the solution is obtained in either a least-squares or minimum-norm sense via a regularized inverse. The realization of either of these solutions results in the statistically optimized portion of SONAH[50]. Regularization essentially filters out high-order wavenumbers associated with non-acoustic measurement noise that would otherwise create significant errors in inward reconstructions. A modified Tikhonov regularization method (see Ref. [51]) is employed to accomplish this. Once the inverse problem has been solved, to propagate out to reconstruction locations, a matrix $\boldsymbol{\alpha}$ is created:

$$\boldsymbol{\alpha} = \begin{bmatrix} \Psi_1(r_{q1}) & \cdots & \Psi_1(r_{qn}) \\ \vdots & \ddots & \vdots \\ \Psi_N(r_{q1}) & \cdots & \Psi_N(r_{qn}) \end{bmatrix}, \tag{6}$$

where n is the number of reconstruction locations. Like the matrix **A**, $\boldsymbol{\alpha}$ serves as a transfer matrix from the reference surface out to various reconstruction locations. The inverse problem can then be leveraged to predict acoustic properties at the reconstruction locations by evaluating the linear equation

$$\boldsymbol{p_q^T} = \boldsymbol{c\alpha} = \boldsymbol{p_h^T R_{A^H A} A^H \alpha}, \tag{7}$$

where $\mathbf{R_{A^H A}}$ is the regularized pseudoinverse of $\mathbf{A^H A}$. Thus, the acoustic behavior at reconstruction locations is obtained from the hologram via a two-step transfer process. The SONAH process shown here is applied to complex acoustic pressure, however, its application can be extended to particle velocity as well, enabling the construction of acoustic intensity[52]. This paper will focus only on the acoustic pressure results.

The SONAH process also involves certain techniques to address a limited-aperture measurement of a partially coherent jet noise source. This process is summarized graphically in Fig. 3. First, synchronously measured time-domain pressure signals across the array are Fourier transformed to create frequency-dependent cross-spectral matrices (CSMs) that contain both amplitude and phase information. Multiple runups of the engine are used to increase the number of blocks to average over in determining CSMs. Second, the field is decomposed into partial, self-coherent

Downloaded by Kent Gee on June 13, 2022 | http://arc.aiaa.org | DOI: 10.2514/6.2022-3028

fields using a singular value decomposition (SVD) method. Third, various enhancements are made to mitigate finite aperture and discrete spatial sampling limitations, such as a numerical aperture extension using an analytic continuation method (see Ref. [53]), interpolation, etc. Fourth, a basis set of selected wavefunctions (a transfer matrix between the hologram and a reference surface) is regularized to select the optimal solution. Fifth, the coefficients of the wavefunctions are determined in either a least-squares or min-norm sense. Once the wavefunctions and their coefficients have been determined, these can be used to reradiate the field to nearly any desired location.

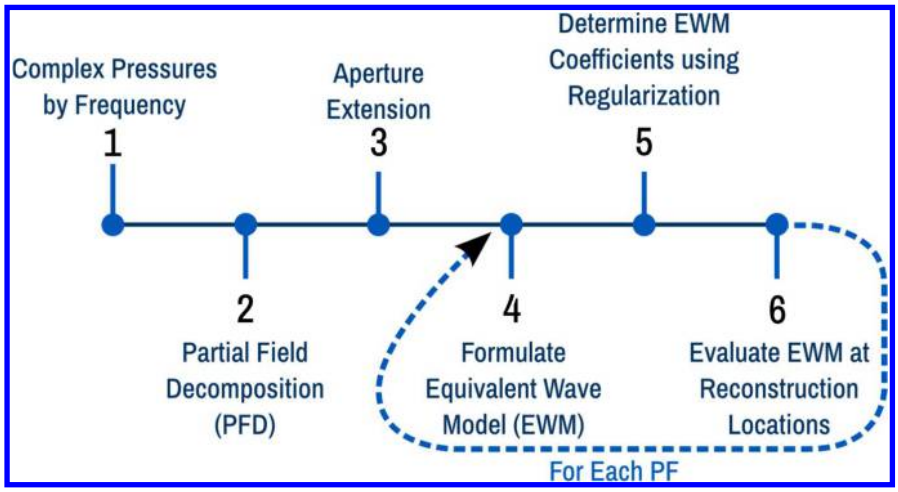

Figure 3. Graphical summary of the SONAH algorithm.

IV. Analysis

A. Partial Field Decomposition

Since jet noise is stochastic/partially-stochastic, ensemble-averaged quantities are typically used in the analysis of the noise. Consequently, the SONAH process on jet noise requires that the signal be separated into partial, self-coherent fields which can yield important insight into the nature of the source. Using SVD to accomplish this partial field decomposition (PFD) results in 120 partial fields arranged in order of energy content. The nature of the SVD-based partial field decomposition results in a non-unique solution with partial fields (PFs) that may not have a direct physical interpretation. Other methods have been proposed to extract PFs with a greater connection to physical sources[54,55]. However, SVD-obtained PFs are useful for understanding the spectral characteristics of coherent "modes" in the signal. Figure 4 shows the partial field amplitude results of the PFD process arranged by partial field number over a span of frequencies for the MIL and AB conditions. Using SVD for the PFD process results in values being arranged by energy, from least to greatest.

For all engine conditions in Figure 4, an 8+ dB separation between the first and second PFs is maintained through low frequencies up to 100 Hz. While this cannot be physically tied to a particular source distribution, it does indicate that there is a single, dominant noise source throughout the low frequency (<100 Hz) regime. As the frequency increases beyond 100 Hz, more PFs are required to represent the total energy. Thus, higher frequency noise is generally represented by several sources incoherent from each other. This is consistent with field analyses of full-scale supersonic jets by Harker *et al.*[56] and Swift *et al.*[57] that show shorter coherence lengths at higher frequencies.

Downloaded by Kent Gee on June 13, 2022 | http://arc.aiaa.org | DOI: 10.2514/6.2022-3028

Downloaded by Kent Gee on June 13, 2022 | http://arc.aiaa.org | DOI: 10.2514/6.2022-3028

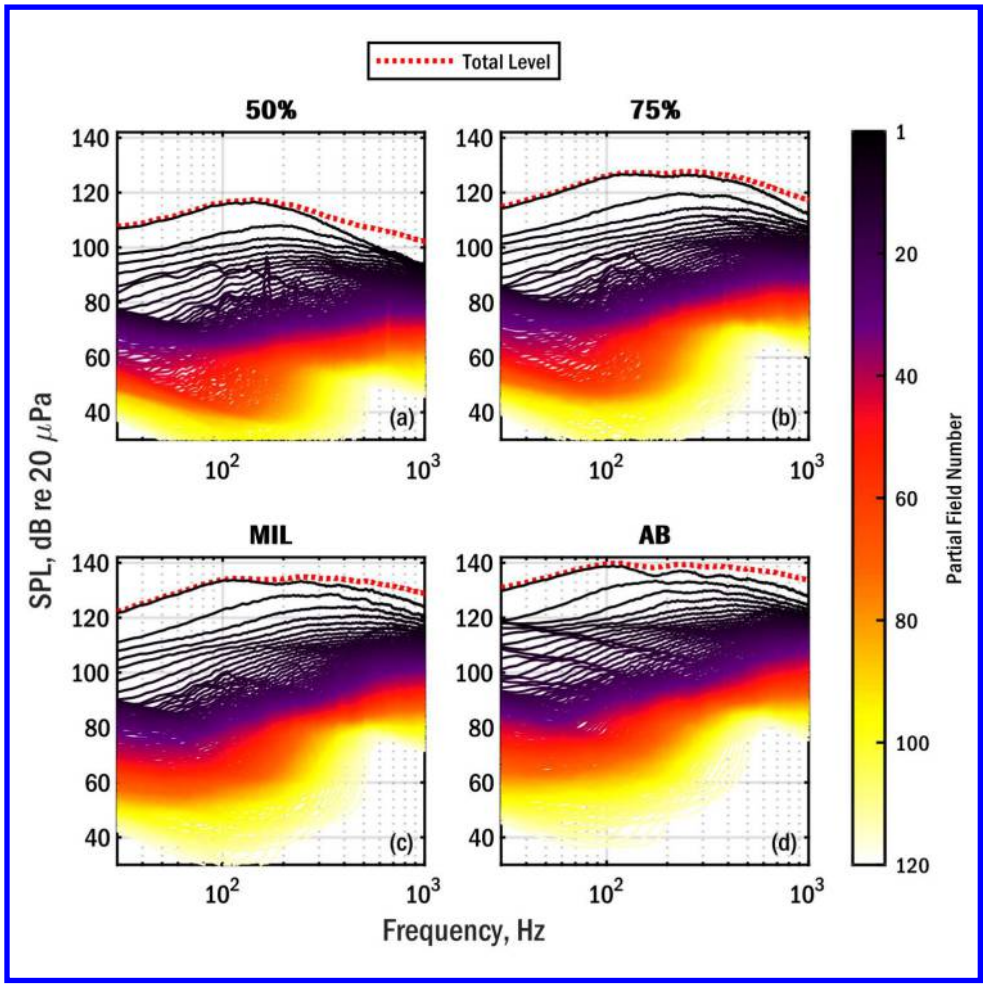

Figure 4. Partial fields by frequency, arranged by partial field number for four engine conditions.

Similar spectral trends for PFDs can be seen for all engine conditions in Fig. 4, albeit with an increase in levels following the increase in thrust, as expected. For 50% thrust, it can be seen in Fig. 4a that at higher frequencies (>500 Hz), the first and second PF become similar in energy, whereas in all three higher conditions, the first and second PFs remain separated by 2+ dB through 1 kHz. Notably, in many of these PFDs, a bump in the partial field amplitudes can be seen around 500+ Hz. This may be due to spatial aliasing in the array, as the entire imaging array has exceeded its design frequencies in this range. However, further investigation into this observation will not be addressed here.

Figure 4d shows the PFD for the AB engine condition. Negative slope (~-20 dB per decade) ripples can be seen in the PFs below 200 Hz. This is likely due to saturation events in some higher-sensitivity microphones around $x =$ 4.6 m (15 ft) in the imaging array during AB measurements, which was addressed by Leete *et al.*[43] Despite initial filtering to reduce saturation effects, they are still visible in these results, although it should be noted that their effects are confined to >10 dB and at most frequencies, >20 dB, below the overall level shown in Fig. 4b. Thus, their effect on reconstructed levels is minimal. Future efforts will investigate further reduction of saturation effects.

Figure 5 shows the number of SVD-derived PFs required to represent 95% (within 0.2 dB) of the total energy in the signal. Through 100 Hz for all conditions, 5 PFs or less comprise greater than 95% of total energy. 50% thrust requires the most PFs to represent the source above ~200 Hz, while AB requires the most below this threshold. This trend for AB is likely due to the saturation effects visible in Fig. 4d. 75% thrust and MIL require fewer partial fields overall than 50% thrust above 200 Hz; however, AB does not follow this trend. Saturation effects impact only lower frequencies, generally below 100 Hz, so it is not a likely culprit for this disparity in MIL. Further examination of the number of partial fields required as a function of engine condition, field location, and frequency will be examined as part of future reduced-order modeling efforts such as those by Wall *et al.*[55] and Harker *et al.*[56].

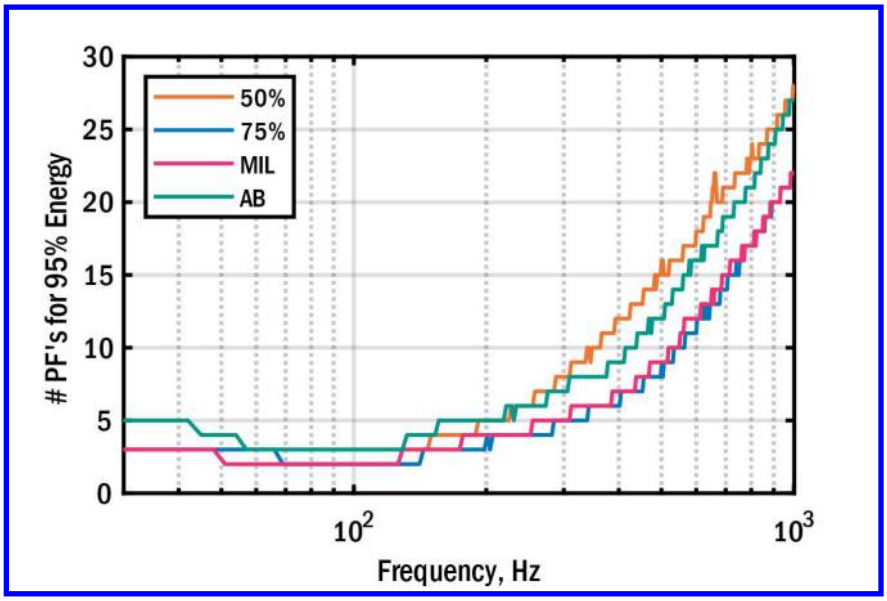

Figure 5. Number of partial fields required to represent 95% of the total energy in the PFD, by frequency. Results are shown for the four considered engine conditions.

B. Source Regions

1. Lipline Reconstructions

The SONAH process is performed on each of the partial fields, and the results are summed energetically to produce total reconstructed levels at each frequency. Figure 6 shows spatiospectral reconstructions along the nozzle lipline ($y = D_e/2$) for four engine conditions between 50% and AB, with amplitude relative to the maximum SPL. A lipline SONAH reconstruction can be seen as analogous to an "equivalent" source. Levels are indicated relative to the global SPL_{max} of each map, which is referenced above each map. This maximum global value increases with engine thrust, with the highest level occurring at AB.

Downloaded by Kent Gee on June 13, 2022 | http://arc.aiaa.org | DOI: 10.2514/6.2022-3028

Downloaded by Kent Gee on June 13, 2022 | http://arc.aiaa.org | DOI: 10.2514/6.2022-3028

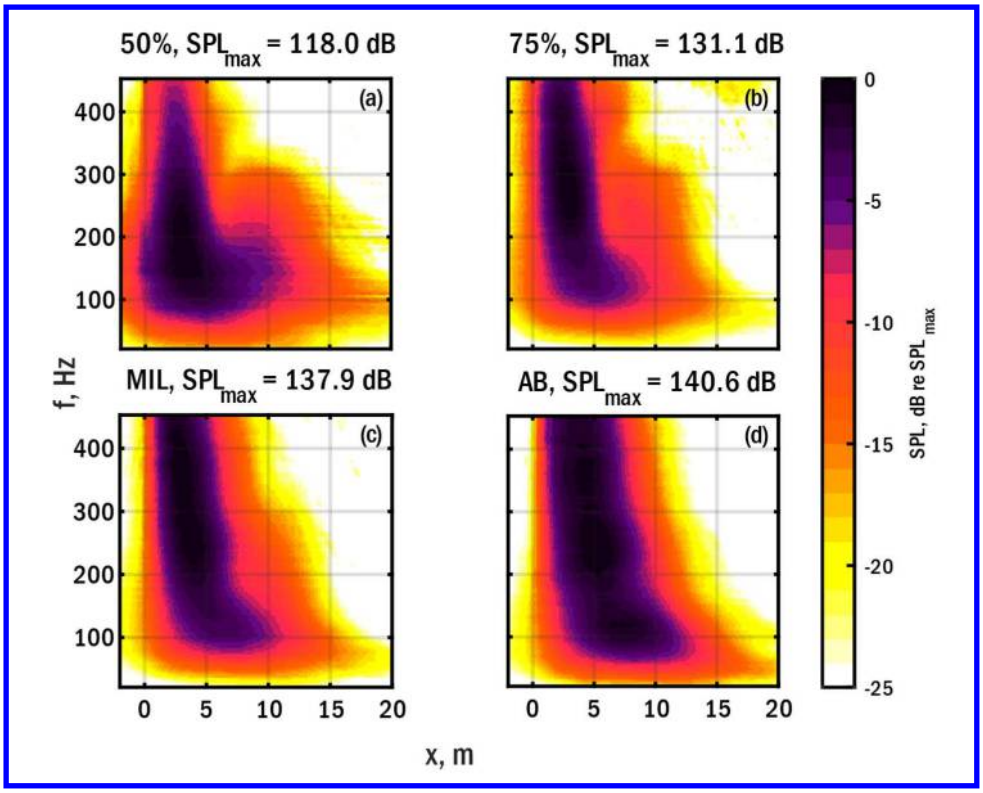

Figure 6. Spatiospectral reconstructions along the nozzle lipline for engine conditions ranging from 50% thrust to AB.

Figure 6a and b distinctly show two separate radiation peaks for a given frequency between approximately 200 and 300 Hz. These two spectral peaks, one higher amplitude and one lower, appear to be centered around 3.5 and 8 m, respectively. Beamforming results by Olaveson *et al.*[58] have ray-traced separate radiation lobes from the same F404 measurement to similar locations along the jet centerline. The higher amplitude peak corresponds to Olaveson *et al.*'s Lobe 2 and the lower amplitude peak corresponds to their Lobe 1. This double-peaked behavior is less visible in these results and in those presented by Olaveson *et al.* at MIL and nearly disappears at AB, however, this may be due to it being "buried" by the higher amplitude noise at MIL and AB.

Figure 7a shows the lipline (x) location of $\mathrm{SPL}_{\max}(f)$. For each engine condition, the location of the maximum shifts upstream with x decreasing linearly with respect to $\log(f)$ throughout the frequency range shown. As thrust increases with engine condition, the location of the maximum shifts downstream. Interestingly, when viewing the width of the -3 dB re $\mathrm{SPL}_{\max}(f)$ (often referred to as full width at half maximum or FWHM) regions in Fig. 7b, they are generally similar for all engine conditions, except the width for AB above ~160 Hz is 1-2 m greater than the other three engine conditions. Comparing with beamforming results from Podboy *et al.*[30], who indicated a location of peak production location of $x/D_e \approx 6.5$ at 300 Hz for AB, Fig. 7a shows a maximum location of $x/D_e \approx 8$. The array in the Podboy *et al.* study was located to the sideline, however, and may have not captured energy being radiated further downstream, which may contribute to the further downstream radiation seen in this study.

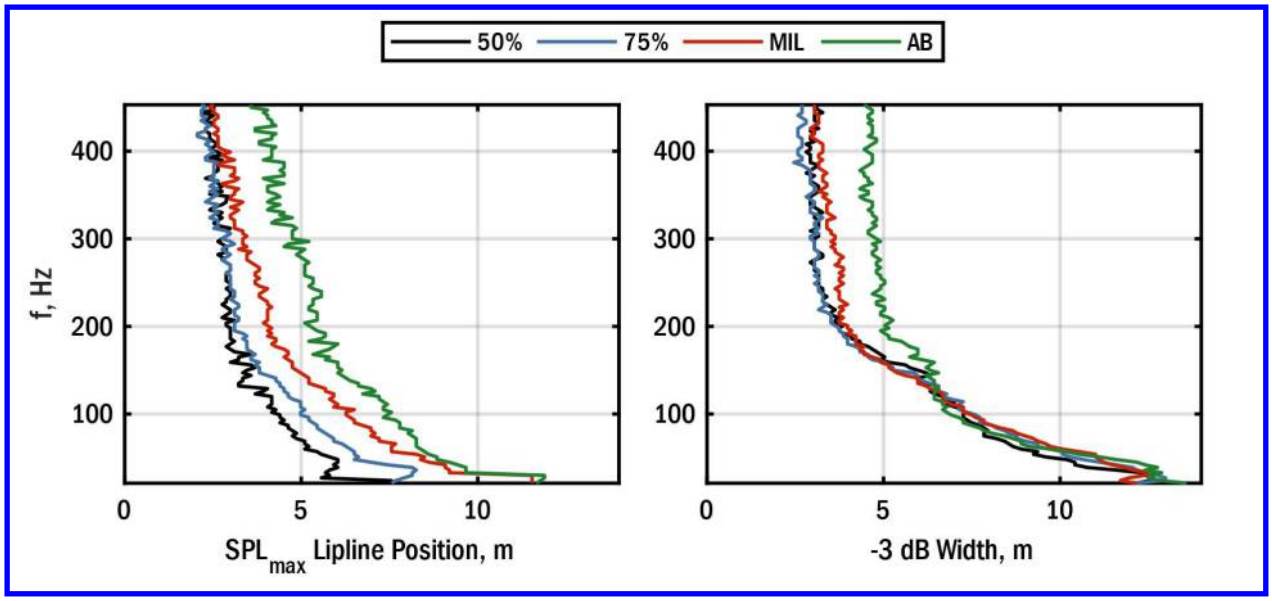

Figure 7. a) Lipline x location of SPL_{max} for each engine condition as a function of frequency. b) Width of -3 dB re SPL_{max} (FWHM) region as a function of frequency.

At the AB condition, the lipline position of SPL_{max} at 400+ Hz is around 3.5-4.5 m (~5.6-7.3 D_e). Comparing with other studies from installed, full-scale, afterburning jets, Harker *et al.*[38] and Wall *et al.*[37] show maxima locations around 4.9-6.0 m (~8.2-10 D_e) for a jet with a rectangular nozzle in a similar frequency range using beamforming and holography, respectively. Leete *et al.*[24] show an apparent source location in this frequency range of ~6 m (~6 D_e) for another full-scale afterburning jet with a round nozzle. While the peak frequencies of these different jets is expected to shift somewhat, this does suggest that these different jets all have similar maxima locations in similar frequency ranges.

2. *AB Relative Maxima*

While Fig. 7a-c show source distributions with relatively smoothly varying amplitudes, Fig. 7d reveals distinct local maxima for AB. Figure 8a repeats the spatiospectral reconstruction along the nozzle lipline for the AB condition, with markers to indicate three local maxima present in the reconstruction and dotted white contours indicating 1 dB down from each local maximum. Relative source maxima such as these have been previously observed in full-scale military jet noise[24,36]. For convenience in discussion, we will refer to the local maxima in Fig. 8 as LM I, LM II, and LM III, ordered from high to low frequency, respectively. Figure 8b shows the spatial distribution of these local maxima, with the upper and lower bounds indicating the spatial extrema of each -1 dB region, and the marker indicating the spatial center of each maximum. Approximate potential and supersonic core lengths are shown, using the Liu *et al.* values for L_c and L_s, with an AB diameter of 0.62 m.

Downloaded by Kent Gee on June 13, 2022 | http://arc.aiaa.org | DOI: 10.2514/6.2022-3028

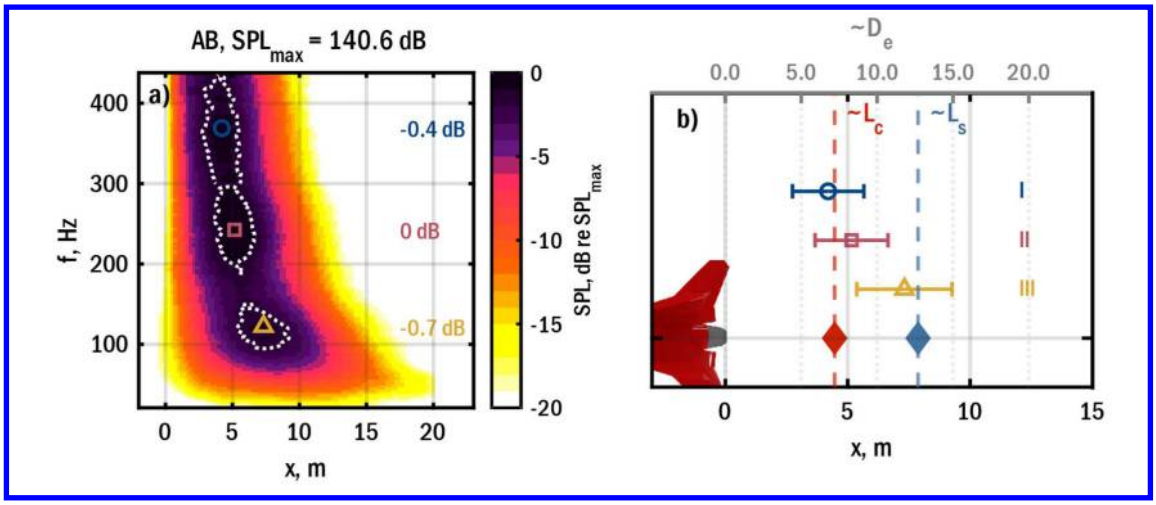

Figure 8. a) Spatiospectral map reconstructed along the nozzle lipline using SONAH at AB. The white dotted contours indicate the -1 dB regions from each indicated local maximum. b) Spatial distribution of three relative source maxima reconstructed along the nozzle lipline. The spatial extent refers to the -1 dB region relative to each local maximum.

The nearly 9 m (~16 D_e) spatial extent of the lower frequencies above -6 dB in Fig. 8a suggests that the region of low-frequency production spans several important regions of the flow, extending from $x/D_e \approx 5$ (upstream of $\sim L_c$) to $x/D_e \approx 19$ around 100 Hz (far downstream of $\sim L_s$). Higher frequencies are generally mapped farther upstream, while lower amplitude, low-frequency noise is present throughout the flow, extending far downstream.

Considering the highlighted maxima in Fig. 8a, we can attempt to connect the relative source maxima to the three acoustically significant flow regions proposed by Leete *et al.*[5], a summary of which is given in Table 1. LM I occurs around 370 Hz centered at a lipline location of $x/D_e \approx 6.8$. If we consider the predictions of Leete *et al.*[5] and others for L_c and L_s to be reasonably accurate for high-temperature-ratio, supersonic jets, then the center of LM I lies just ahead of L_c and higher frequency noise is generated upstream of this location, corresponding to Leete *et al.*'s flow region 1. Likewise, for LM II centered near 240 Hz and $x/D_e \approx 8.3$, this also follows Leete *et al.*'s flow region 2. Continuing to LM III centered near 120 Hz and $x/D_e \approx 11.8$, this is near the third suggested source region downstream of L_s, albeit slightly farther upstream. Thus, these data agree well with the three source regions proposed, with the greatest variation seen around LM III. Of note is that the centers of these three LMs appear quasi-harmonic in frequency, although no attempt is made here to explain this observation.

Applying the attributed noise components from Leete *et al.*[5] in Table 1, it is suggested that LM I is primarily responsible for MWR throughout the shear layer and LM II may be tied to slowing Mach waves in the decelerating region of the flow beyond L_c. Mechanistically, this may suggest that LM I and II may be tied to more Kelvin-Helmholtz-type instabilities as discussed by Schmidt *et al.*[25]. The attribution of a specific source mechanism to LM III is less straightforward. Whereas LM I and II are tightly grouped around the potential core tip and are likely tied primarily to MWR, beyond L_c a strict transition to LSN is unlikely. Portions of the flow between L_c and L_s still contain convectively supersonic structures, resulting in MWR, however, developed large-scale structure are likely also present, leading to an amalgamation of phenomena. Thus, LM III likely contains portions of MWR from decelerating yet convectively supersonic turbulence, with LSN also present. This region may contain both Kelvin-Helmoltz-type instabilities and Orr-type waves discussed by Schmidt *et al.*[25], however, further investigation is required to make any definitive conclusion on this hypothesis. While it should be noted that these results are preliminary and associated only through comparison, this does indicate that the acoustic source of the F404 may be separable into three primary source regions that individually contribute to radiated noise through different mechanisms.

Comparing these source localization results with the groupings of Vaughn *et al.*[13] (See Table 1), LM I and LM II seem to correspond with Vaughn *et al.*'s group 3, attributed to MWR. For the AB condition, group 3 was localized (for the 5th and 95th percentiles) to between $x/D_e \approx 2.5$ and $x/D_e \approx 9.7$, while the -1 dB distributions for local maxima I and II shown in Fig. 8b span approximately $x/D_e \approx 4.4$ to $x/D_e \approx 10.7$. Groups 4-6 from Vaughn *et al.*, attributed to LSN, were localized to between $x/D_e \approx 6.5$ and $x/D_e \approx 14.6$, compared to local maximum III from Fig. 8b spanning $x/D_e \approx 8.7$ to $x/D_e \approx 15.0$. However, this region of flow is shown by Vaughn *et al.* to contain multiple groups of

Downloaded by Kent Gee on June 13, 2022 | http://arc.aiaa.org | DOI: 10.2514/6.2022-3028

radiation with differing directivities and phenomenological groupings. Thus, LM III may contain both LSN and MWR, while LM I and LM II both be principally associated with MWR.

Table 1. Summary of important regions discussed. All locations are reported in approximate nozzle diameters. Noise components attributed to spatial regions are noted. Similar spatial distributions across studies are grouped by row. Each analysis refers to an AB or AB-like condition.

T-7A				**Leete *et al.*[5] (LES)**			**Vaughn *et al.*[13] (Full Scale)**				
Local Max.	-1 dB	Center	-1 dB	Flow Region	Location	Attrib. Noise	Group(s)	5%	Mean	95%	Attrib. Noise
LM I	4.4	6.8	9.1	1	≤7.2	MWR	3	2.5	7	9.7	MWR
LM II	5.9	8.3	10.7	2	7.2-12.7	MWR, LSN					
LM III	8.7	11.8	15	3	≥12.7	LSN	4,5,6	6.5-8.3	9.6-11.0	12.8-14.6	LSN

The local maximum with the highest amplitude is LM II (by about 0.4 dB), which seems to emanate downstream of L_c, but upstream of L_s. This is consistent with Potter[16] and Nagamatsu *et al.*[17], who suggested that the region of greatest sound power production in a supersonic jet exists between L_c and L_s. However, LM I is only 0.4 dB lower, and there is considerable overlap between the spatial distributions of LM I and LM II, thus it is sufficient to say that the area of maximum amplitude resides around L_c, which is more consistent with the findings of Leete *et al.*[22]. Additionally, Greska *et al.*[59] suggested that the maximum level of a lab-scale supersonic jet originated from the end of the potential core. While a full sound power analysis is beyond the scope of this particular paper, the observation of significant levels that appear to originate from this region in this dataset seems consistent with historical theory and findings. Analyses to calculate sound power production along the length of the jet from the holography results will be the subject of future work.

V. Conclusions

In conclusion, the application of SONAH to an installed F404-GE-103 engine has indicated many significant properties of the acoustic source. PFD results show a single dominant, coherent noise source below 100 Hz for engine conditions ranging from 50% thrust to AB. 95% of the total energy at these frequencies can be represented by 5 or fewer SVD-derived partial fields. Two distinct source maxima are readily visible at 50% and 75% thrust at frequencies ranging between 200 and 300 Hz. This indicates that at certain frequencies, multiple distinct areas in the flow may be contributing significantly to radiated sound. Additionally, three distinct relative local maxima (LM) are present in the lipline spatiospectral reconstructions for AB. While the comparisons made between observed LM at AB are strictly phenomenological, they do indicate that there are three separate relative source maxima for the F404, which span different spatial regions and which occupy distinct frequency ranges. Through comparison with other studies, each of these maxima likely contribute to acoustic radiation through different source mechanisms; LM I and II may primarily radiate as MWR, while LM III be comprised of both MWR and LSN. Further investigation into these local maxima and radiation mechanism may yield further insight into the origin of noise in supersonic jets.

Acknowledgments

The authors gratefully acknowledge the Office of Naval Research for funding under grant number N00014-21-1-2069 with project monitor Dr. Steven Martens, Code 351 Jet Noise Reduction. The measurements were funded through the Advanced Pilot Training System Program Office and the Air Force Research Laboratory. Distribution A: Approved for public release; distribution unlimited. Cleared 05/26/20222; 43-9693-22

References

[1] Ffowcs Williams, J. E. "The Noise from Turbulence Convected at High Speed." *Philosophical Transactions of the Royal Society of London. Series A, Mathematical and Physical Sciences*, Vol. 255, No. 1061, 1963, pp. 469–503. https://doi.org/10.1098/rsta.1963.0010.

[2] Nagamatsu, H. T., and Horvay, G. Supersonic Jet Noise. 1970.

[3] Tam, C. K. W. "Supersonic Jet Noise." *Annu. Rev. Fluid Mech*, Vol. 27, 1995, pp. 17–43. https://doi.org/10.1146/annurev.fl.27.010195.000313.

Downloaded by Kent Gee on June 13, 2022 | http://arc.aiaa.org | DOI: 10.2514/6.2022-3028

[4] Bailly, C., and Fujii, K. "High-Speed Jet Noise." *Mechanical Engineering Reviews*, Vol. 3, No. 1, 2016, pp. 15-00496-15–00496. https://doi.org/10.1299/mer.15-00496.

[5] Leete, K. M., Gee, K. L., Liu, J., and Wall, A. T. "Coherence Analysis of the Noise from a Simulated Highly Heated Laboratory-Scale Jet." *AIAA Journal*, Vol. 58, No. 8, 2020, pp. 3426–3435. https://doi.org/10.2514/1.j059112.

[6] Chen, S., Gojon, R., and Mihaescu, M. "Flow and Aeroacoustic Attributes of Highly-Heated Transitional Rectangular Supersonic Jets." *Aerospace Science and Technology*, Vol. 114, 2021. https://doi.org/10.1016/j.ast.2021.106747.

[7] Tang, G., Chen, Y., Silaen, A. K., Wang, T., and Zhou, C. Q. "Investigation of Supersonic Oxygen Jet Potential Core Length at Various Ambient Temperatures." *JOM*, Vol. 71, No. 2, 2019, pp. 633–643. https://doi.org/10.1007/s11837-018-3244-y.

[8] Baars, W. J., Murray, N. E., and Tinney, C. E. "A Proper Framework for Studying Noise from Jets with Non-Compact Sources." *Journal of Fluid Mechanics*, Vol. 929, 2021, p. A23. https://doi.org/10.1017/jfm.2021.837.

[9] Liu, J., Johnson, R. F., and Ramamurti, R. Numerical Study of Supersonic Jet Noise Emanating from an F404 Nozzle at Model Scale. 2019.

[10] Tam, C., Golebiowski, M., and Seiner, J. On the Two Components of Turbulent Mixing Noise from Supersonic Jets. 1996.

[11] Tam, C. K. W., Viswanathan, K., Ahuja, K. K., and Panda, J. "The Sources of Jet Noise: Experimental Evidence." *Journal of Fluid Mechanics*, Vol. 615, 2008, pp. 253–292. https://doi.org/10.1017/S0022112008003704.

[12] Viswanathan, K. Investigation of the Sources of Jet Noise. 2007.

[13] Vaughn, A. B., Gee, K. L., Swift, S. H., Leete, K. M., Wall, A. T., Downing, J. M., and James, M. M. "Source Localization of Crackle-Related Events in Military Aircraft Jet Noise." *AIAA Journal*, Vol. 59, No. 6, 2021, pp. 2251–2261. https://doi.org/10.2514/1.j059823.

[14] Liu, J., Corrigan, A., Kailasanath, K., and Taylor, B. Impact of the Specific Heat Ratio on the Noise Generation in a High-Temperature Supersonic Jet. No. 0, 2016.

[15] Prasad, C., and Morris, P. J. "Steady Active Control of Noise Radiation from Highly Heated Supersonic Jets." *The Journal of the Acoustical Society of America*, Vol. 149, No. 2, 2021, pp. 1306–1317. https://doi.org/10.1121/10.0003570.

[16] Potter, R. C. *An Investigation to Locate the Acoustic Sources in a High Speed Jet Exhaust Stream*. 1968.

[17] Nagamatsu, H. T., Sheer, R. E. , Jr., and Horvay, G. Supersonic Jet Noise Theory and Experiments. 1969.

[18] Eldred, K. M. *Acoustic Loads Generated by the Propulsion System*. 1971.

[19] Gee, K. L. "A Tale of Two Curves and Their Influence on Rocket and Supersonic Jet Noise Research." *The Journal of the Acoustical Society of America*, Vol. 149, No. 4, 2021, pp. 2159–2162. https://doi.org/10.1121/10.0003938.

[20] Liu, J., Corrigan, A., Kailasanath, K., and Gutmark, E. Impact of Chevrons on Noise Source Characteristics in Imperfectly Expanded Jet Flows. 2015.

[21] Liu, J., Kailasanath, K., and Gutmark, E. Similarity Spectral Analysis of Highly Heated Supersonic Jets Using Large-Eddy Simulations. 2017.

[22] Leete, K. M., Gee, K. L., Liu, J., and Wall, A. T. "Near-Field Acoustical Holography and Acoustic Power Analysis of a Simulated, Highly Heated Supersonic Jet." *The Journal of the Acoustical Society of America*, Vol. 151, No. 3, 2022, pp. 1989–2001. https://doi.org/10.1121/10.0009827.

[23] Liu, J., Kailasanath, K., Munday, D., and Gutmark, E. Investigation of Near-Field Acoustic Properties of Imperfectly Expanded Jet Flows Using LES. 2009.

Downloaded by Kent Gee on June 13, 2022 | http://arc.aiaa.org | DOI: 10.2514/6.2022-3028

[24] Leete, K. M., Wall, A. T., Gee, K. L., Neilsen, T. B., James, M. M., and Downing, J. M. "Acoustical Holography-Based Analysis of Spatiospectral Lobes in High-Performance Aircraft Jet Noise." *AIAA Journal*, Vol. 59, No. 10, 2021, pp. 4166–4178. https://doi.org/10.2514/1.j059400.

[25] Schmidt, O. T., Towne, A., Rigas, G., Colonius, T., and Brès, G. A. "Spectral Analysis of Jet Turbulence." *Journal of Fluid Mechanics*, Vol. 855, 2018, pp. 953–982. https://doi.org/10.1017/jfm.2018.675.

[26] Seiner, J. M., Ukeiley, L. S., and Jansen, B. J. *Aero-Performance Efficient Noise Reduction for the F404-400 Engine*. 2005.

[27] Greska, B., Krothapalli, A., Seiner, J. M., Jansen, B., and Ukeiley, L. The Effects of Microjet Injection on an F404 Jet Engine. No. 5, 2005, pp. 3051–3073.

[28] Greska, B., and Krothapalli, A. On the Far-Field Propagation of High-Speed Jet Noise. 2008.

[29] Murray, N. E., and Jansen, B. J. "Performance Efficient Jet Noise Reduction for Supersonic Nozzles." *International Journal of Aeroacoustics*, Vol. 11, Nos. 7 & 8, 2012, pp. 937–956.

[30] Podboy, G. G., Bridges, J. E., and Henderson, B. S. *Phased Array Noise Source Localization Measurements of an F404 Nozzle Plume at Both Full and Model Scale*. 2010.

[31] Tam, C. K. W., Aubert, A. C., Spyropoulos, J. T., and Powers, R. W. "On the Dominant Noise Components of Tactical Aircraft: Laboratory to Full Scale." *Journal of Sound and Vibration*, Vol. 422, 2018, pp. 92–111. https://doi.org/10.1016/j.jsv.2018.02.023.

[32] Tam, C. K. W., and Parrish, S. A. "Noise of High-Performance Aircraft at Afterburner." *Journal of Sound and Vibration*, Vol. 352, 2015, pp. 103–128. https://doi.org/10.1016/j.jsv.2015.04.010.

[33] Wall, A. T., Gee, K. L., James, M. M., Bradley, K. A., McInerny, S. A., and Neilsen, T. B. "Near-Field Noise Measurements of a High-Performance Military Jet Aircraft." *Noise Control Engineering Journal*, 2012, pp. 421–434.

[34] Seiner, J. M., Jansen, B. J., and Ukeiley, L. S. Acoustic Fly-Over Studies of F/A-18 E/F Aircraft During FCLP Mission. 2003.

[35] Seiner, J. M., Ukeiley, L. S., and Jansen, B. J. Noise Reduction Technology for F/A-18 E/F Aircraft. 2004.

[36] Schlinker, R. H., Liljenberg, S. A., Polak, D. R., Post, K. A., Chipman, C. T., and Stern, A. M. Supersonic Jet Noise Source Characteristics & Propagation: Engine and Model Scale. 2007.

[37] Wall, A. T., Gee, K. L., Neilsen, T. B., McKinley, R. L., and James, M. M. "Military Jet Noise Source Imaging Using Multisource Statistically Optimized Near-Field Acoustical Holography." *The Journal of the Acoustical Society of America*, Vol. 139, No. 4, 2016, pp. 1938–1950. https://doi.org/10.1121/1.4945719.

[38] Harker, B. M., Gee, K. L., Neilsen, T. B., Wall, A. T., and James, M. M. "Source Characterization of Full-Scale Tactical Jet Noise from Phased-Array Measurements." *The Journal of the Acoustical Society of America*, Vol. 146, No. 1, 2019, pp. 665–680. https://doi.org/10.1121/1.5118239.

[39] Stout, T. A., Gee, K. L., Neilsen, T. B., Wall, A. T., and James, M. M. "Source Characterization of Full-Scale Jet Noise Using Acoustic Intensity." *Noise Control Engineering Journal*, Vol. 63, No. 6, 2015, pp. 522–536.

[40] van Komen, D. F., Harker, B. M., Neilsen, T. B., Gee, K. L., Hales Swift, S., Wall, A. T., Micah Downing, J., and James, M. M. "Characterizing Distinct Components of Tactical Aircraft Noise Sources." *The Journal of the Acoustical Society of America*, Vol. 147, No. 5, 2020, pp. 3550–3564. https://doi.org/10.1121/10.0001260.

[41] Ennix, K. A., Burcham, F. W., and Webb, L. D. *Flight-Determined Engine Exhaust Characteristics of an F404 Engine in an F-18 Airplane*. 1993.

[42] Seiner, J. M., Ukeiley, L. S., and Jansen, B. J. Aero-Performance Efficient Noise Reduction for the F404-400 Engine. 2005.

[43] Leete, K. M., Vaughn, A. B., Bassett, M. S., Rasband, R. D., Novakovich, D. J., Gee, K. L., Campbell, S. C., Mobley, F. S., and Wall, A. T. Jet Noise Measurements of an Installed Ge F404 Engine. 2021.

Downloaded by Kent Gee on June 13, 2022 | http://arc.aiaa.org | DOI: 10.2514/6.2022-3028

[44] Shah, P. N., Vold, H., and Yang, M. Reconstruction of Far-Field Noise Using Multireference Acoustical Holography Measurements of High-Speed Jets. 2011.

[45] Lee, M., and Bolton, J. S. "Source Characterization of a Subsonic Jet by Using Near-Field Acoustical Holography." *The Journal of the Acoustical Society of America*, Vol. 121, No. 2, 2007, pp. 967–977. https://doi.org/10.1121/1.2404626.

[46] Long, D., Peters, J., and Anderson, M. Evaluating Turbofan Exhaust Noise and Source Characteristics from Near Field Measurements. 2009.

[47] Wall, A. T., Gee, K. L., and Neilsen, T. B. "Multisource Statistically Optimized Near-Field Acoustical Holography." *The Journal of the Acoustical Society of America*, Vol. 137, No. 2, 2015, pp. 963–975. https://doi.org/10.1121/1.4906585.

[48] Hald, J. "Basic Theory and Properties of Statistically Optimized Near-Field Acoustical Holography." *The Journal of the Acoustical Society of America*, Vol. 125, No. 4, 2009, pp. 2105–2120. https://doi.org/10.1121/1.3079773.

[49] Leete, K. M., Wall, A. T., Gee, K. L., Neilsen, T. B., Harker, B. M., and James, M. M. Azimuthal Coherence of the Sound Field in the Vicinity of a High Performance Military Aircraft. No. 29, 2016.

[50] Steiner, R., and Hald, J. "Near-Field Acoustical Holography without the Errors and Limitations Caused by the Use of Spatial DFT." *International Journal of Acoustics and Vibration*, Vol. 6, No. 2, 2001, pp. 83–89. https://doi.org/10.20855/ijav.2001.6.278.

[51] Williams, E. G. "Regularization Methods for Near-Field Acoustical Holography." *The Journal of the Acoustical Society of America*, Vol. 110, No. 4, 2001, pp. 1976–1988. https://doi.org/10.1121/1.1404381.

[52] Stout, T. A., Wall, A. T., Gee, K. L., and Neilsen, T. B. Obtaining Acoustic Intensity from Multisource Statistically Optimized Near-Field Acoustical Holography. No. 33, 2018.

[53] Williams, E. G. "Continuation of Acoustic Near-Fields." *The Journal of the Acoustical Society of America*, Vol. 113, No. 3, 2003, pp. 1273–1281. https://doi.org/10.1121/1.1528173.

[54] Kim, Y.-J., Bolton, J. S., and Kwon, H.-S. "Partial Sound Field Decomposition in Multireference Near-Field Acoustical Holography by Using Optimally Located Virtual References." *The Journal of the Acoustical Society of America*, Vol. 115, No. 4, 2004, pp. 1641–1652. https://doi.org/10.1121/1.1642627.

[55] Wall, A. T., Gee, K. L., Leete, K. M., Neilsen, T. B., Stout, T. A., and James, M. M. "Partial-Field Decomposition Analysis of Full-Scale Supersonic Jet Noise Using Optimized-Location Virtual References." *The Journal of the Acoustical Society of America*, Vol. 144, No. 3, 2018, pp. 1356–1367. https://doi.org/10.1121/1.5053580.

[56] Harker, B. M., Gee, K. L., Neilsen, T. B., Wall, A. T., and James, M. M. Beamforming-Based Wavepacket Model for Noise Environment Predictions of Tactical Aircraft. 2017.

[57] Swift, S. H., Gee, K. L., Neilsen, T. B., Wall, A. T., Downing, J. M., and James, M. M. Spatiotemporal Correlation Analysis of Jet Noise from a Round-Nozzle Supersonic Aircraft. 2018.

[58] Olaveson, T., Ward, J. A., Johnson, J. P., Gee, K. L., and Wall, A. T. Analysis of Spatiospectral Lobes in Installed F404 Engine Noise Radiation. 2022.

[59] Greska, B., Krothapalli, A., Horne, W. C., and Burnside, N. "A Near-Field Study of High Temperature Supersonic Jets." *14th AIAA/CEAS Aeroacoustics Conference (29th AIAA Aeroacoustics Conference)*, No. May, 2008, pp. 5–7. https://doi.org/10.2514/6.2008-3026.

Downloaded by Kent Gee on June 13, 2022 | http://arc.aiaa.org | DOI: 10.2514/6.2022-3028